In Situ Thermal Preparation of Polyimide Nanocomposite Films Containing Functionalized Graphene Sheets

ARTICLE *in* ACS APPLIED MATERIALS & INTERFACES · NOVEMBER 2010

Impact Factor: 6.72 · DOI: 10.1021/am1008437 · Source: PubMed

3 AUTHORS, INCLUDING:

Tianxi Liu
Fudan University
233 PUBLICATIONS **7,189** CITATIONS

SEE PROFILE

ARTICLE

In Situ Thermal Preparation of Polyimide Nanocomposite Films Containing Functionalized Graphene Sheets

Dan Chen, Hong Zhu, and Tianxi Liu*

Key Laboratory of Molecular Engineering of Polymers of Ministry of Education, Department of Macromolecular Science, Fudan University, Shanghai 200433, P. R. China

ABSTRACT Graphene oxides (GO) were exfoliated in N,N-dimethylformamide by simple sonication treatment of the as-prepared high quality graphite oxides. By high-speed mixing of the pristine poly(amic acid) (PAA) solution with graphene oxide suspension, PAA solutions containing uniformly dispersed GO can be obtained. Polyimide (PI) nanocomposite films with different loadings of functionalized graphene sheets (FGS) can be prepared by in situ partial reduction and imidization of the as-prepared GO/PAA composites. Transmission electron microscopy observations showed that the FGS were well exfoliated and uniformly dispersed in the PI matrix. It is interesting to find that the FGS were highly aligned along the surface direction for the nanocomposite film with 2 wt % FGS. Tensile tests indicated that the mechanical properties of polyimide were significantly enhanced by the incorporation of FGS, due to the fine dispersion of high specific surface area of functionalized graphene nanosheets and the good adhesion and interlocking between the FGS and the matrix.

KEYWORDS: polyimide • nanocomposites • functionalized graphene sheets • in situ reduction • orientation

INTRODUCTION

Aromatic polyimides (PI) are considered to be one of the most important high performance materials in microelectronics and aircraft industries because of their superior mechanical properties, excellent thermal stability, high glass transition temperature, and good resistance to solvents (1−4). However, with the rapid development in some special applications, such as spacecraft and aircraft industries, the mechanical, electrical, and thermal properties of PI films are not good enough to meet the extreme requirements. In recent years, increasing attention has been paid to the polyimide based organic/inorganic hybrid materials. It was found that the mechanical, thermal and anticorrosive properties of PI films were significantly improved by the incorporation of a small amount of nanofillers (5−9).

Over recent years, polymer nanocomposites containing layered filler materials were intensively studied because the nanoplatelets can improve stiffness/toughness balance, heat distortion temperature, flame proofing, and abrasion resistance of the matrices (10−12). As a member of the carbon family, graphene has attracted much attention since the experimental discovery in 2004 for its dazzling electronic and mechanical properties (13−16). As a novel two-dimensional material, graphene is essentially a carbon nanotube cut along its axis and unrolled to lay flat. Since natural graphite is still abundant, it is highly cost-effective with respect to the synthetic carbon nanotubes when functionalized graphenes are derived from graphite. Functionalized graphene sheets (FGS) serve as fillers for the enhancement of mechanical and electrical properties in composite materials, where the key issue is to achieve a good dispersion with an exfoliated morphology (16−18). It was found that through a rapid high temperature (varied from 300 to 1100 °C) thermal expansion of graphite oxides, FGS can be obtained (14−20). Giannelis et al., Jeong et al,. and Steurer et al. prepared a series of FGS based polymer nanocomposites and investigated the morphological and physical properties of these nanomaterials (16, 17, 20). However, all these nanocomposites containing FGS were prepared by the mechanical mixing of the as-prepared FGS with polymers, which are not beneficial for the uniform dispersion of FGS in the polymer matrix. As the functional groups of graphene oxide (GO) were partially removed during the high temperature treatment process, the interfacial interactions between the polymer and the FGS are not strong enough for effective load transfer from the matrix to the nanosheets, as well as uniform dispersion of the FGS, which are the crucial problems for the fabrication of high performance nanocomposites. Compared with FGS, GO, which possesses lots of carboxylate, hydroxyl and epoxide groups on the surfaces, can be much easily dispersed and exfoliated in polar solvents. Preparation of monolayer GO dispersed nanocomposites and subsequent in situ reduction of GO is considered as an effective method to fabricate FGS hybrid materials with maximum interfacial interaction between the FGS and the matrix (21, 22).

The well-developed synthetic method of polyimide is the two-step method, which consists of the synthesis of poly-

* To whom correspondence should be addressed. Tel: +86-21-55664197. Fax: +86-21-65640293. E-mail: txliu@fudan.edu.cn.

Received for review September 7, 2010 and accepted November 2, 2010

DOI: 10.1021/am1008437

Published on Web 11/10/2010

(amic acid) (PAA, the precursor of polyimide) and subsequent thermal imidization (at about 300 °C) of PAA (2, 10, 23, 24). Herein, we described a facile method for the preparation of FGS/PI nanocomposites by utilizing GO/PAA composites as the precursors because we found that GO can be partially reduced to FGS during the high-temperature imidization process. By imidization and a simultaneous partial in situ reduction of the as-prepared GO/PAA composites, PI nanocomposites containing uniformly dispersed FGS can be successfully obtained. Both the modulus and the tensile strength of the synthesized FGS/PI nanocomposites were significantly improved compared with neat PI, due to homogeneous dispersion and good orientation of FGS in the matrix.

EXPERIMENTAL SECTION

Materials. Pyromellitic dianhydride (PMDA), 4,4′-oxidianiline (ODA), *N*,*N*-dimethylformamide (DMF), 37% HCl, 98% H_2SO_4, 30% H_2O_2, $KMnO_4$, and $NaNO_3$ were commercially obtained from China Medicine Co. Natural graphite powder (325 mesh) was supplied by Alfa-Aesar. All reactants were analytical purity and used as received.

Synthesis of Pristine Poly(amic acid) Solution. The precursor of polyimide, PAA, was synthesized from PMDA and ODA with an equivalent molar ratio. The polycondensation was performed in DMF at a temperature of about 0 °C, and the solid content of the pristine PAA solution was 25%.

Preparation of Graphene Oxide and Its Exfoliated Suspension. A modified Hummers method was utilized to synthesize oxidized graphite powder (25). Typically, 2.5 g of natural graphite, 2.5 g of $NaNO_3$, and 7.5 g of $KMnO_4$ were slowly added to 50 mL of concentrated H_2SO_4 under vigorous stirring below 5 °C. Then the mixture was stirred continuously for 1 h at 35 °C to oxidize the graphite. After that, 100 mL water was added into the mixture, and the temperature was increased to higher than 90 °C, and the suspension was maintained at 95−100 °C for 15 min. Then, the mixture was poured into 300 mL of deionized water, after that 20 mL of H_2O_2 was added into the suspension. After cooling to room temperature, the solid products were filtered, subsequently washed with 5% HCl aqueous solution and water, and finally dried to obtain graphite oxide.

The obtained graphite oxide was dispersed in DMF (1.0 mg mL^{-1}) by ultrasonication treatment by using an ultrasonication bath cleaner for 3 h. The resulting exfoliated GO suspension was centrifuged at 2000 rpm for 5 min to remove the unexfoliated graphite oxide particles.

Preparation of PI and its Nanocomposites Containing FGS. Neat PI and PI/FGS films were prepared by conventional solution casting method and subsequent thermal imidization. For preparation of neat PAA solution used for film casting, viscous pristine PAA solution was diluted by DMF, and for GO/PAA solutions, the pristine PAA solution was diluted by the mixture of DMF and GO/DMF (1 mg mL^{-1}) suspension. As an example, 10 mL of GO suspension and 10 mL of DMF were added to 4 g of pristine PAA solution by mechanical stirring at 5 °C for 6 h to obtain 1 wt % GO/PAA solution. Neat and 2 wt % PAA solutions were prepared by solution mixing of the pristine PAA solution with 20 mL of DMF or 20 mL of GO suspension.

All the cast films were first dried at 60 °C for 4 h to remove the residual solvent and then thermally imidized via the following procedure to complete the imidization process: (1) heating up to 100 °C at a rate of 3 °C min^{-1} and then annealing there for 30 min, (2) heating up to 200 °C at a rate of 3 °C min^{-1} and annealing there for 30 min, and (3) heating up to 300 °C at a rate of 3 °C min^{-1} and annealing there for 30 min. During the above high-temperature thermal imidization process, the GO nanosheets can be partially in situ reduced to FGS, thus obtaining the FGS/PI nanocomposite films directly.

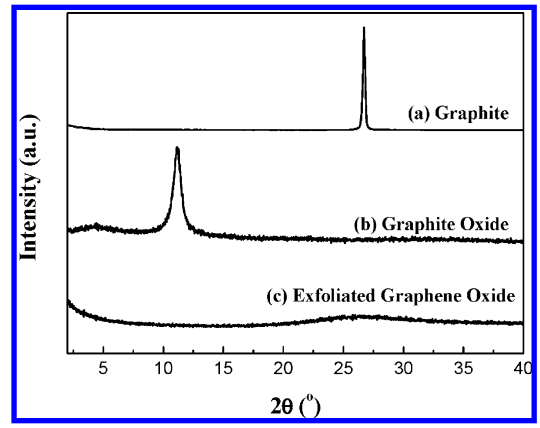

FIGURE 1. XRD patterns of (a) graphite, (b) graphite oxide, and (c) the aggregate obtained by centrifugation from colloidal suspension of exfoliated GO nanosheets.

Characterization. X-ray diffraction (XRD) experiments were conducted on a PANalytical (X′Pert PRO) X-ray diffractometer using Cu Kα radiation ($\lambda = 0.154$ nm) at an accelerating voltage of 40 kV and current of 40 mA. The surface topography and the thickness of GO nanosheets deposited onto mica wafers were examined using a NanoScope IV atomic force microscopy (AFM) from Digital Instruments. Raman spectra were measured on LabRam-1B French Dilor Com ($\lambda_{ex} = 632.8$ nm). Transmission electron microscopy (TEM) observations of the GO/PI nanocomposite films were performed under an acceleration voltage of 200 kV with a Philips CM 300 FEG TEM. Thin sections (with a thickness below 100 nm) for TEM observations were cut from the as-prepared composites under cryogenic conditions using a Leica ultramicrotome with a diamond knife. Tensile tests of the film samples were carried out using an Instron universal material testing system, and the samples were directly mounted to the sample clamps and stretched at a speed of 5 mm min^{-1}. Tensile property values reported here represent an average of the results for tests run on at least five samples. Scanning electron microscope (SEM, Tescan) performed at an acceleration voltage of 20 kV was used to observe the morphology of GO, FGS, and the fractured surfaces of the neat PI and its nanocomposite samples. Thermogravimetric analysis (Pyris 1 TGA) was performed under nitrogen flow at a heating rate of 20 °C min^{-1}.

RESULTS AND DISCUSSION

Novel carbon-based nanostructures are intensively investigated as high performance nanofillers in the polymer nanocomposite field. The challenges in the area of organic/inorganic hybrid materials are to achieve significant improvements in the interfacial adhesion between the matrix and the reinforcing fillers. In this study, GO was utilized as the nanofiller precursor because it possesses lots of functional groups on the surface, which are potentially beneficial for the interactions with PAA precursor or PI matrix. Figure 1a and b show the XRD curves of graphite and graphite oxide. It can be seen that the intense and sharp peak of natural graphite at $2\theta = 26.7°$ shifted to 11.1°, indicating the incorporation of various functional groups. Generally speaking, the sharper the XRD peak, the higher crystallinity the sample has. The expanded XRD peak (larger full width

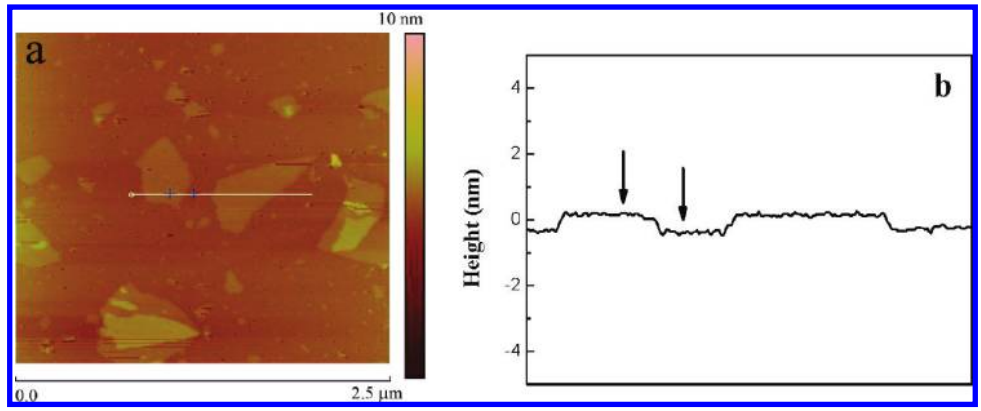

FIGURE 2. AFM image of GO exfoliated in DMF.

at half-maximum of XRD peak than that of graphite) of the oxidized graphite indicated a decreased crystallinity of the oxidized graphite. Figure S1, Supporting Information, shows the Raman spectra of graphite and graphite oxide. The typical features in the Raman spectra are the G band (about 1586 cm^{-1}) and the D band (about 1350 cm^{-1}). The intensity ratio of D and G bands (I_D/I_G) is a measure of the extent of disorder. It can be seen that the graphite was successfully oxidized.

To demonstrate that the graphite oxide can be partially reduced to FGS during the high temperature imidization process, the graphite oxide samples were experienced the same thermal treatment as the imidization process. Figure S2a and S2b, Supporting Information, show the SEM micrographs of graphite oxide and the FGS prepared by the high-temperature exfoliation of graphite oxide. The wrinkled structure of the FGS can be clearly observed, indicating an exfoliation by the imidization process. That is, after the thermal treatment, graphite oxides were exfoliated because of the pyrolysis of carboxyl and hydroxyl groups, which evolved into the interstices between the graphene sheets during heating process. Figure S3, Supporting Information, shows the XRD curve of the obtained FGS. The absence of any diffraction peak indicates the collapse of the ordered layer structure. The XRD and SEM results indicate that the graphite oxides can be successfully exfoliated into FGS during the high-temperature imidization process. Besides that, the color of the graphite oxide powder was changed from brown to black (not shown here for short) because of the pyrolysis of functional groups, which indicated again the partial reduction of graphite oxides during the high temperature treatment. Figure S4, Supporting Information, shows the TGA curves of graphite oxide and FGS. It can be seen that graphite oxide showed a significant weight loss below 300 °C because of the pyrolysis of carboxyl and hydroxyl groups. The as-prepared FGS showed considerable improved thermal stability because of the reduced functional groups. Figure S1, Supporting Information, shows the Raman spectra of graphite oxide and FGS. The I_D/I_G was decreased from 1.36 to 1.11, which indicated the partial reduction of GO to FGS.

The XRD, SEM, and macroscopic results indicate that the graphite oxide can be successfully expanded and partially reduced to FGS. In comparison to conventional graphite oxide, the expanded FGS possesses much higher degree of exfoliation, higher specific surface areas, and less defect. However, as most of the functional groups of FGS were removed during the high temperature reduction process, it is not easy to obtain the polymer nanocomposites with uniform FGS dispersion. Moreover, some expanded or exfoliated graphite oxides might restore to the layered graphite structure during the fabrication of polymer nanocomposites. Thus, preparation of single layer GO dispersed nanocomposites and subsequent in situ partial reduction of the GO to FGS is thought to be the most efficient method to fabricate FGS hybrid materials with maximum interfacial bonding between FGS and the matrix. In this study, we prepared monolayer FGS dispersed polyimide nanocomposite films by utilizing the well exfoliated graphene oxide nanosheets as precursor nanofillers.

It has been reported that graphite oxides can be exfoliated and well dispersed in DMF by increasing the sonication time (26). In this study, single layer GO nanosheets were prepared by ultrasonication of the well oxidized graphite oxide in DMF. It should be noted that the successful oxidization of graphite is crucial for the exfoliation of graphene oxides. The XRD curve of the gel-like aggregate freshly obtained by centrifugating the GO suspension for 30 min at 30 000 rpm is shown in Figure 1c. It can be seen that the diffraction peak of graphite oxide at $2\theta = 11.1°$ disappeared, indicating a complete exfoliation of graphite oxide. The very broad halo in the 2θ range of 20−30° was attributed to the scattering of DMF within the gel-like aggregate of GO. Figure 2a and b display the tapping-mode AFM image of the exfoliated GO nanosheets by depositing the DMF suspension on a mica substrate. As shown in Figure 2b, the height profile measurement (by scanning along the marked white line in Figure 2a) indicated that the crystallite terrace was rather flat with an average thickness of about 0.6 nm, indicating a successful delamination of graphite oxide in DMF.

To eliminate the influence of molecular weight on the mechanical properties of the PI nanocomposites and investigate how the FGS incorporation influences the properties of PI films, the casting solutions (0−2 wt % FGS) were prepared by high speed mixing the pristine PAA solution with DMF or the GO/DMF solutions. By the in situ imidization

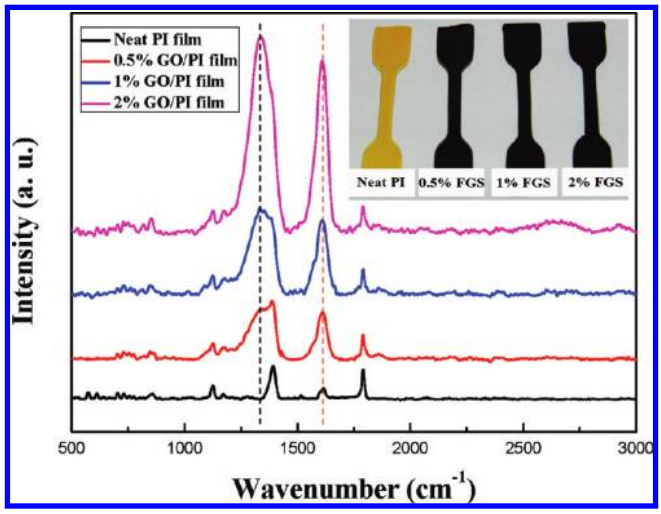

FIGURE 3. Raman spectra of neat polyimide and its nanocomposites with different FGS loadings.

and simultaneous in situ partial reduction of GO, single-layer FGS dispersed polyimide nanocomposite films can be obtained.

Raman spectroscopy is a powerful probe for characterizing carbonaceous materials. Figure 3 shows the Raman spectra of neat PI and its nanocomposites with different FGS loadings. It can be clearly seen that the intensity of the D band (about 1356 cm^{-1}) and G band (about 1586 cm^{-1}) of the nanocomposites was gradually increased with the increase of FGS content. The 2D Raman band at ~2700 cm^{-1} can be clearly observed for the sample with 2 wt % FGS, which indicated the partial reduction of graphene oxides. The weak and broad peak at about 2930 cm^{-1} can be attributed to the defects or the "disorder-induced" bands of the graphene sheets (27). The inset graph shows the digital photographs of neat PI and its nanocomposites with different FGS loadings. One can see that, the color of the nanocomposite films containing FGS was black rather than brown (the color of graphite oxide). With incorporation of only 0.5 wt % FGS, the transparent PI film became rather dark, compared with the yellow neat PI film, which indicates the uniform dispersion of FGS nanosheets in the PI matrix. With the increase of the FGS content, the color of the films became darker and darker. Thus, we can conclude that the GO nanosheets simultaneously experience a partial reduction process upon high temperature imidization.

As is known that the homogeneous dispersion of nanofillers in polymeric matrices is one of the most important factors for fabricating high-performance composites. TEM was employed here to observe the dispersion state of the FGS fillers in the nanocomposites. The TEM images (Figure 4a and b) of the ultrathin sections of the nanocomposite films containing 1 and 2 wt % FGS show a fine dispersion of FGS in the PI matrix. In these micrographs the aligned graphene platelets appear as distinct dark lines homogeneously dispersed in the matrix. One can clearly see that the majority of FGS particles has been successfully exfoliated in the matrix and the functionalized graphene nanosheets were uniformly dispersed throughout the polymeric matrix. It could be expected that the functional groups on the surfaces

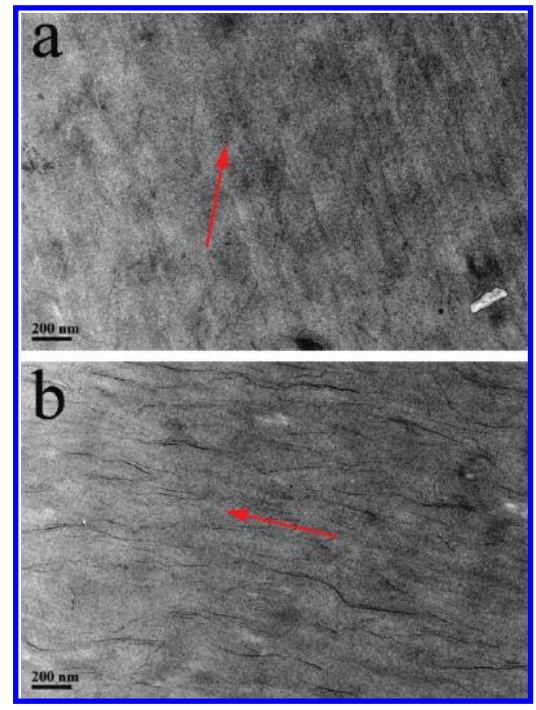

FIGURE 4. TEM micrographs of 1 wt % FGS/PI and 2 wt % FGS/PI nanocomposite films.

and sides of GO nanosheets may form hydrogen bonds with the C═O groups on the polymer chains of PAA or PI, as reported in the case of acid-modified carbon nanotubes (23). In this study, the strong interactions between the carboxyl, hydroxyl or epoxy groups of the GO and the PAA (the N and O along the PAA chains) may also lead to the homogeneous dispersion of GO in the PAA matrix (28). Besides that, the carboxyl groups on the graphene surfaces or edges may react with the amido of PAA during the high-temperature imidization process (as shown in Scheme S1, Supporting Information). The formation of PI grafted graphene nanosheets is critical for the uniform dispersion of FGS in the matrix, as well as the strong interfacial interactions between them.

It is interesting to find that the nanosheets were oriented along the film surface dierction (as indicated by the red arrows in Figure 4), especially for the nanocomposite film with 2 wt % FGS. As shown in Scheme 1, the FGS nanosheets with high aspect ratios might be preferentially aligned along the nanocomposite film surfaces due to the solution flow and solvent evaporation during the solution casting process. The FGS nanoplateles were inclined to lay flat during the solution casting process because of their high aspect ratio, that is, flow induced orientation of FGS. During solvent evaporation process, the thickness of the films became thinner and thinner, thus the graphene nanosheets may be mainly deposited or oriented along the film surface. Besides that, the thickness confinement effect may be another key factor for the good alignment of FGS nanosheets in the nanocomposite films. As the thickness of the films was about 30−40 μm, whereas the lateral sizes of graphene nanosheets are larger than several hundred nanometers, the graphene nanosheets tend to be spontaneously aligned along the film surface direction. It seems from the TEM results that with the increase of the graphene sheet contents (e.g., from 1 to

Scheme 1. Schematic Showing the Possible Orientation Mechanism of FGS in the Polyimide Nanocomposite Films during Solution Casting Process

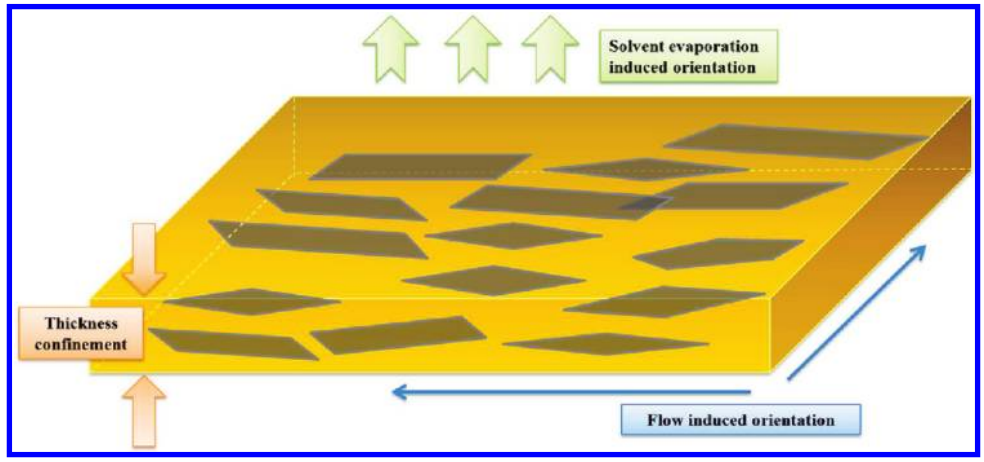

2 wt %), the orientation degree of FGS was increased. This is probably because the higher graphene content in the nanocomposite films, the more compact for the FGS stacks, and the more distinct for the thickness confinement effect induced FGS orientation.

Typical stress–strain curves of neat PI and the PI/FGS composites are shown in Figure 5, and the tensile properties are summarized in Table 1. As expected, one can see that by the incorporation of only 0.5 wt % FGS, the tensile strength and modulus of polyimide were significantly increased. This reinforcement effect from FGS can be mainly attributed to its fine dispersion and high orientation in PI, as well as the efficient load transfer from the matrix to FGS nanoparticles, because of the strong interfacial interactions between them. It can be seen that the elongation at break

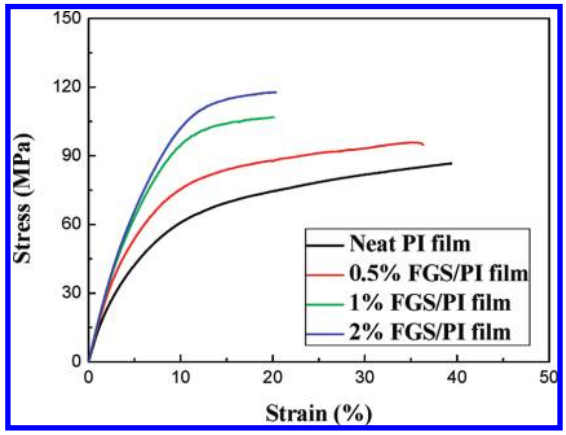

FIGURE 5. Typical stress–strain curves of neat PI and FGS/PI nanocomposites.

Table 1. Summary of Mechanical Properties of the PI Nanocomposites as a Function of FGS Concentration

film samples	tensile strength (MPa)	tensile modulus (GPa)	elongation at break (%)
neat PI	88.4 ± 17.6	1.29 ± 0.15	39.3 ± 9.2
0.5% FGS/PI	99.2 ± 15.4	1.56 ± 0.25	35.2 ± 8.6
1% FGS/PI	107.8 ± 13.2	1.62 ± 0.21	20.0 ± 6.1
2% FGS/PI	118.5 ± 12.2	1.68 ± 0.18	20.1 ± 6.3

for the 0.5 wt % FGS/PI sample was only slightly decreased, indicating that a small amount of FGS did not lead to the brittleness of polyimide. Further increasing the FGS contents, the tensile strength was increased gradually. Upon the incorporation of 1 wt % FGS, however, the tensile elongation was decreased significantly, probably because the FGS loading exceeds the critical level (maybe 0.5 wt %). The excess FGS may form small agglomerates (e.g., some dark dots in Figure 4a), which play a role of stress concentration sites, thus becoming one of the possible origins of the embrittlement of the nanocomposites. Another possible reason is that FGS acts as physical cross-linking points in the matrix and restricts the movement or mobility of polymer chains thus leading to the brittleness of the composites. It is interesting to find that the tensile toughness of 2 wt % FGS/PI sample is comparable with that of the 1 wt % one. We assume that this can be ascribed to the increased alignment of FGS in the 2 wt % sample. The films with higher FGS orientation may lead to better FGS dispersion. As shown in Figure 4b, the nanoplatelets were evenly distributed in the matrix, and almost no aggregates were observed. Besides, the aligned nanoplatelets in the nanocomposites may serve as connecting bridges to prevent the polymer matrix from fracturing upon mechanical deformation.

To better understand the tensile properties of the PI/FGS nanocomposites, the fractured surfaces upon tensile testing were observed by SEM, as shown in Figure 6. It can be seen that, under lower magnification, the fractured surface of neat PI was rather flat and smooth (Figure 6a). The bright dots and lines (as shown by the red arrows in Figure 6b) indicated that the PI matrix was stretched out upon mechanical deformation. For the PI composite with 0.5 wt % FGS, the fractured surface (Figure 6c) was relatively rough, compared with that of neat PI film. The SEM micrograph at high magnification for the fractured surface of 0.5 wt % FGS/PI was shown in Figure 6d. As indicated by the red arrows, the tough surface upon fracture can be attributed to the strong interfacial adhesion and good compatibility between the FGS and the matrix, thus being favorable to stress transfer from the polymer matrix to the FGS nanofillers. The fractured

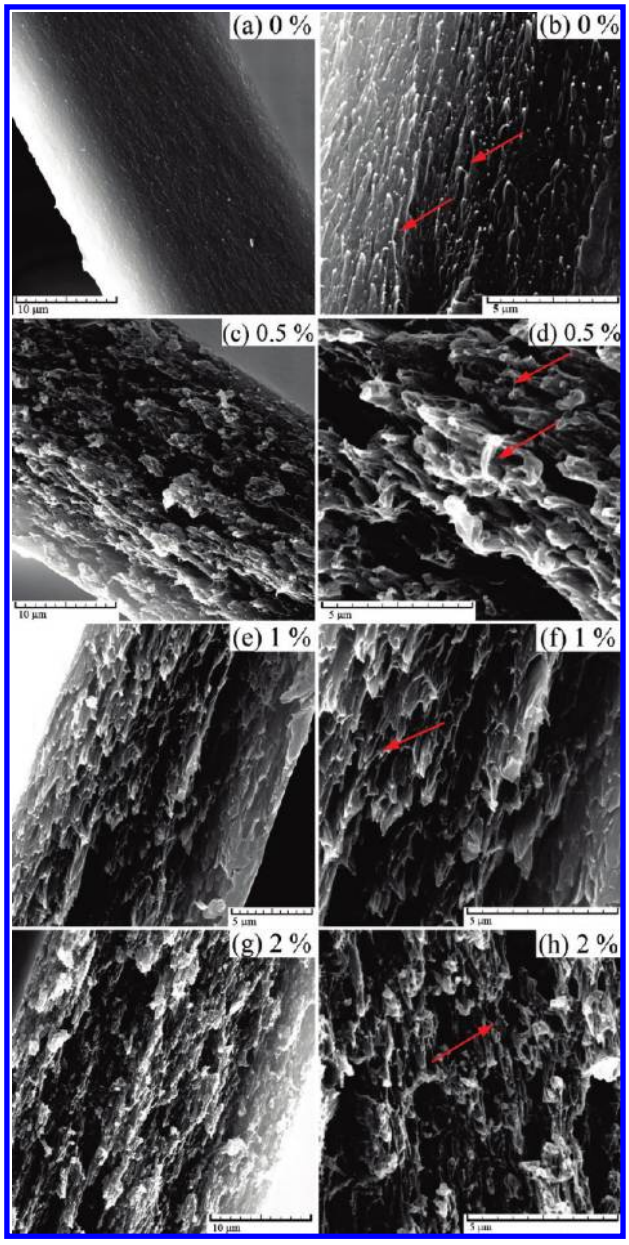

FIGURE 6. SEM micrographs of the fractued surfaces of neat PI and its nanocomposites containing different FGS loadings.

surfaces became somewhat brittle with the increase of FGS loading level, which is consistent with the tensile tests. And it can be clearly seen that the FGS were uniformly dispersed in the matrix, as indicated by the red arrows in Figure 6e–h. Therefore, the finely dispersed FGS throughout the polymeric matrix and the strong interaction between the nanofillers and the matrix are responsible for the significant reinforcement of the mechanical properties of the PI/FGS nanocomposite films prepared.

Thermal stability is one important property for PI-based nanocomposites as they are potentially used as high-performance engineering plastics. The thermal properties of PIs are usually improved by the addition of inorganic additives. As shown in Figure 7, the thermal stability (e.g., the 5% weight loss temperature) of polyimide was improved slightly by the incorporation of FGS. Although the carboxyl or hydroxyl groups introduced into the graphene sheets are

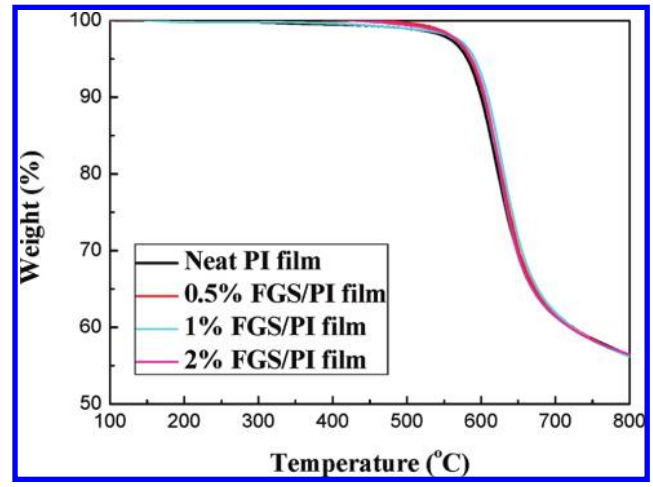

FIGURE 7. TGA curves of neat PI and its nanocomposites containing FGS.

easily decomposed at high temperature and may serve as catalysts for the degradation of PI and thus deteriorate the thermal stability of PI matrix, the thermal stability of the nanocomposites was no worse than that of neat PI. Hence, in situ partial (thermal) reduction after incorporating graphene oxides into the PAA matrix is a facile method to fabricate high performance FGS/PI nanocomposite films. The significant improvement of mechanical properties of polyimide can be attributed to the fine dispersion of high aspect ratio FGS and strong interfacial adhesion and interlocking structure between the graphene and the matrix, arising from the wrinkled morphology of FGS.

CONCLUSIONS

We have demonstrated that graphite oxides can be partially reduced to functionalized graphene sheets during the preparation process of polyimide under high-temperature imidization treatment condition. By exfoliating the graphite oxides in DMF and subsequent high-speed mixing with the pristine PAA solution, PAA solutions with uniformly dispersed GO can be obtained. Polyimide nanocomposite films with different FGS loadings can be prepared by the in situ reduction and imidization of the as-prepared GO/PAA composites. TEM and SEM results showed that the FGS were well exfoliated and uniformly dispersed in the PI matrix. The mechanical properties (such as tensile strength and modulus) of polyimide were improved significantly by the incorporation of highly aligned FGS. Our study develops a facile and effective way to fabricate high performance polyimide nanocomposite films containing functionalized graphene sheets.

Acknowledgment. This work was supported by the National Natural Science Foundation of China (20774019; 50873027), "Shu Guang" project (09SG02) supported by Shanghai Municipal Education Commission, and Shanghai Education Development Foundation.

Supporting Information Available: Raman spectra of graphite, graphite oxide, and FGS; SEM micrographs of graphite oxide and FGS; XRD curve of FGS prepared by the

thermal exfoliation of graphite oxides; TGA curves of graphite oxide and FGS; and schematic of the reaction that might happen between graphene oxide and PAA during the high temperature imidization process (PDF). This material is available free of charge via the Internet at http://pubs.acs.org.

REFERENCES AND NOTES

(1) Hasegawa, T.; Horie, K. *Prog. Polym. Sci.* **2001**, *26*, 259–335.
(2) Sazanov, Y. N. *Russian J. Appl. Chem.* **2001**, *74*, 1253–1269.
(3) Ge, J. J.; Zhang, D.; Li, Q.; Hou, H. Q.; Graham, M. J.; Dai, L. M.; et al. *J. Am. Chem. Soc.* **2005**, *127*, 9984–9985.
(4) Bin, Y. Z.; Oishi, K.; Koganemaru, A.; Zhu, D.; Matsuo, M. *Carbon* **2005**, *43*, 1617–1627.
(5) Yuen, S. M.; Ma, C. C. M.; Chiang, C. L.; Teng, C. C.; Yu, Y. H. *J. Polym. Sci. Part A, Polym. Chem.* **2008**, *46*, 803–816.
(6) Chen, D.; Liu, T. X.; Zhou, X. P.; Tjiu, W. C.; Hou, H. Q. *J. Phys. Chem. B* **2009**, *113*, 9741–9748.
(7) Lee, T.; Park, S. S.; Jung, Y. I.; Han, S.; Han, D.; Kim, I.; et al. *Eur. Polym. J.* **2009**, *45*, 19–29.
(8) Murugaraj, P.; Mainwaring, D. E.; Mora-Huertas, N. *Compos. Sci. Technol.* **2009**, *69*, 2454–2459.
(9) Lebron-Colon, M.; Meador, M. A.; Gaier, J. R.; Sola, F.; Scheiman, D. A.; McCorkle, L. S. *ACS Appl. Mater. Interfaces* **2010**, *2*, 669–676.
(10) Hsueh, H. B.; Chen, C. Y. *Polymer* **2003**, *44*, 1151–1161.
(11) Zhang, Y. H.; Fu, S. Y.; Li, R. K. Y.; Wu, J. T.; Li, L. F.; Ji, J. H.; et al. *Compos. Sci. Technol.* **2005**, *65*, 1743–1748.
(12) Dong, W. F.; Zhang, X. H.; Liu, Y. Q.; Wang, Q. G.; Gui, H.; Gao, H. M.; et al. *Polymer* **2006**, *47*, 6874–6879.
(13) McBride, J. R.; Lupini, A. R.; Schreuder, M. A.; Smith, N. J.; Pennycook, S. J.; Rosenthal, S. J. *ACS Appl. Mater. Interfaces* **2009**, *1*, 2886–2892.
(14) Verdejo, R.; Barroso-Bujans, F.; Rodriguez-Perez, M. A.; De Saja, J. A.; Lopez-Manchado, M. A. *J. Mater. Chem.* **2008**, *18*, 2221–2226.
(15) Schniepp, H. C.; Li, J. L.; McAllister, M. J.; Sai, H.; Herrera-Alonso, M.; Adamson, D. H.; et al. *J. Phys. Chem. B* **2006**, *110*, 8535–8539.
(16) Ansari, S.; Giannelis, E. P. *J. Polym. Sci. Part B, Polym. Phys.* **2009**, *47*, 888–897.
(17) Steurer, P.; Wissert, R.; Thomann, R.; Mulhaupt, R. *Macromol. Rapid Commun.* **2009**, *30*, 316–327.
(18) Ramanathan, T.; Abdala, A. A.; Stankovich, S.; Dikin, D. A.; Herrera-Alonso, M.; Piner, R. D.; et al. *Nat. Nanotechnol.* **2008**, *3*, 327–331.
(19) Bon, S. B.; Valentini, L.; Verdejo, R.; Fierro, J. L. G.; Peponi, L.; Lopez-Manchado, M. A.; et al. *Chem. Mater.* **2009**, *21*, 3433–3438.
(20) Nguyen, D. A.; Lee, Y. R.; Raghu, A. V.; Jeong, H. M.; Shin, C. M.; Kim, B. K. *Polym. Int.* **2009**, *58*, 412–417.
(21) Liang, J. J.; Huang, Y.; Zhang, L.; Wang, Y.; Ma, Y. F.; Guo, T. Y.; et al. *Adv. Funct. Mater.* **2009**, *19*, 2297–2302.
(22) Vickery, J. L.; Patil, A. J.; Mann, S. *Adv. Mater.* **2009**, *21*, 2180–2184.
(23) Yuen, S. M.; Ma, C. C. M.; Lin, Y. Y.; Kuan, H. C. *Compos. Sci. Technol.* **2007**, *67*, 2564–2573.
(24) Agag, T.; Koga, T.; Takeichi, T. *Polymer* **2001**, *42*, 3399–3408.
(25) Hummers, W. S.; Offeman, R. E. *J. Am. Chem. Soc.* **1958**, *80*, 13391340?.
(26) Paredes, J. I.; Villar-Rodil, S.; Martı´nez-Alonso, A.; Tascon, J. M. D. *Langmuir* **2008**, *24*, 10560–10564.
(27) Livneh, T.; Haslett, T. L.; Moskovits, M. *Phys. Rev. B* **2002**, *66*, 195110–195116.
(28) Zhu, B. K.; Xie, S. H.; Xu, Z. K.; Xu, Y. Y. *Compos. Sci. Technol.* **2006**, *66*, 548–554.

AM1008437